

Linear unmixing with a minimum of spectral bands for fluorescence microscopy images

Ela Claridge¹ and Dale J. Powner²

¹School of Computer Science, The University of Birmingham B15 2TT, U.K.

²Institute for Cancer Studies, The University of Birmingham, Birmingham B15 2TT, U.K.

Abstract— By tagging two or more proteins with different fluorochromes it is possible to study their interactions. The most common method for isolating contributions from the individual fluorochromes is linear spectral unmixing where it is assumed that the characteristic spectra of the contributing fluorochromes are known and that a compound spectrum is a linear combination of the known ‘library’ spectra. Linear unmixing methods commonly use spectral vectors of a relatively large dimension. This paper demonstrates that for resolving N fluorescent compounds it is sufficient to have N spectral measurements acquired at the optimally chosen wavelengths. This is demonstrated on a simulated data corrupted by Poisson noise, on multispectral images of fluorescent beads and on images of cells transfected with fluorescent proteins CFP and GFP. The abundance coefficients for three fluorescent components obtained using images acquired at three optimal wavelengths show excellent correspondence with the coefficients derived using full spectral data acquired at 30 wavelengths. This reduction in the number of wavelengths leads to less bleaching and supports dynamic studies. The only additional processing required for this method is the computation of the optimal wavelengths, which takes the order of minutes and needs to be done only once for a given set of the library spectra and a given imaging system.

I. INTRODUCTION

A major goal of human biomedical research is concerned with determining the causes of disease. A disease of a specific tissue, for example breast cancer, results from a malfunction of some, or all, of the different types of cells that make up that tissue. At the level of the malfunctioning cells, the cause of the disease can be traced to abnormal messages between the different components contained within cells. By mapping the differences in intracellular messages produced by normal and diseased cells we may understand the causes of disease at a fundamental level and subsequently be able to prevent disease formation or develop a strategy for successfully treating the disease.

Intracellular messages are propagated through often multiple direct interactions between various different components within cells, such as protein to protein or protein to lipid interactions, and it is often these interactions that occur abnormally in diseased cells. A key tool in the biologist’s armoury in mapping intracellular messages is the ability to fluorescently tag specific components within a living cell. Different fluorescent tags (fluorochromes) have different

characteristic emission spectra which they produce in response to stimulation by light at an appropriately chosen wavelength. By tagging two or more components with different fluorochromes it is possible to determine the kinetics of their movement through the cell, their coincident localisation within a specific region of the cell and thus their potential to interact and propagate a message. Furthermore, fluorescent resonance energy transfer (FRET) between the appropriately chosen fluorochromes can be used as an indication of direct interaction between components and thus of message propagation.

A major drawback of the techniques using multiple fluorochromes is that often their spectra overlap. This makes the detection of each component alone unreliable when using conventional fluorescent microscope systems. One way around this problem is to ‘unmix’ the emission from each fluorochrome in a sample cell. This technique involves using multispectral imaging to measure the intensity of fluorescent emissions at multiple points in the spectrum; subsequently, by comparing the shape of the obtained spectrum to those of reference spectra for each fluorochrome within the sample cell, it is possible to determine the contribution of each fluorochrome to the image.

The number of wavelength measurements required to build up a spectrum reliable enough for successful unmixing can be several seconds to minutes. However, often the rate at which intracellular components move around the cell is more rapid than this and thus this technique is generally not very useful for obtaining detailed kinetics of components in live cells. Here we have developed a technique that overcomes this problem by more rapidly, but equally reliably, detecting multiple fluorochromes in a living cell by using far fewer specific wavelength measurements.

II. BACKGROUND

A. Principles of fluorescence imaging

When stimulated with light at an appropriate excitation wavelength, fluorochromes (fluorescent proteins or dyes) emit light with a characteristic spectral profile (the emission spectrum). Standard fluorescence microscopes use a complex illumination and optical filter system which directs the

excitation light at a sample containing a fluorochrome and allows only the emission light to reach the viewport and / or an imaging sensor. If more than one fluorochrome needs to be imaged in the same sample, multiple image captures are necessary, each with a different filter set. This set-up is not ideal for dynamic studies or for multiple fluorochromes with overlapping emission spectra, or when it is impossible to totally filter out contributions from the excitation spectra.

Multispectral imaging can overcome some of these difficulties. Instead of recording only light transmitted through an emission filter (a bandpass filter, typical bandwidth 20-40nm), all of the emitted light is allowed to proceed to an imaging sensor. The emitted spectrum is then build up sequentially, by acquiring images at single wavelengths and forming a full multispectral image (sometimes referred to as a lambda-stack or a spectral cube). Alternatively, in a more expensive equipment, 4-10 bands can be simultaneously captured on a set of PMT boards, but with the loss of intensity at each band as the remitted light flux is sub-divided. The contributions from individual fluorochromes can then be determined from a compound spectrum, which will also have unwanted contributions from cell autofluorescence and background fluorescence [1] [3].

B. Linear spectral unmixing

The most common method for isolating the individual contributions is linear spectral unmixing [2]. This assumes that the characteristic spectra, the library spectra, of the contributing fluorochromes are known and that a compound spectrum is a linear combination of the library spectra.

More formally, let K be the number of spectral measurements (wavelengths λ_k at which the images are acquired); let N be the number of fluorochromes (or, more generally, fluorescent compounds), each with its characteristic library spectrum $\mathbf{I}^{(n)}$, $n=1, \dots, N$; and M be the number of samples (pixels in the image). A multispectral image \mathbf{I} comprises $K \times M$ spectral measurements in total. A spectrum \mathbf{s} at any given pixel has contributions from N library spectra with a coefficient a_n describing the relative abundance of $\mathbf{I}^{(n)}$:

$$\mathbf{s} = \mathbf{L} \cdot \mathbf{a} \quad (1)$$

where \mathbf{s} is a column vector of K spectral measurements, \mathbf{L} is a $K \times N$ matrix of N K -dimensional library spectra $\mathbf{I}^{(n)}$ and \mathbf{a} is an N -dimensional column vector of abundance coefficients. Similarly,

$$\mathbf{I} = \mathbf{L} \cdot \mathbf{A} \quad (2)$$

in which case \mathbf{A} is a $N \times M$ matrix $[a_{nm}]$.

Given than $K \geq N$, linear unmixing can solve the equation (2) with respect to \mathbf{A} , i.e. it can recover the relative abundance of each of the library spectrum at each pixel; when $K=N$ by a simple inversion:

$$\mathbf{A} = \mathbf{L}^{-1} \cdot \mathbf{I} \quad (3)$$

It should be noted that there also exist unmixing methods which do not require the explicit knowledge of the library spectra, e.g. [1][3]; there the contributing 'library' spectra are predicted from training samples using e.g. Independent Component Analysis [4], or Real Component Analysis [3].

III. LINEAR UNMIXING USING THE MINIMUM NUMBER OF SPECTRAL BANDS

Most published and commercially available linear unmixing methods use spectral vectors of relatively large dimension, $K \gg N$. However, it can be noted from the equations (2)-(3) that for resolving N fluorescent compounds it is sufficient to have $K=N$ spectral measurements. Provided that the wavelengths λ_k are appropriately chosen, the above system can be solved with N spectral measurements.

A. Selection of spectral bands

A generic method for the optimal selection of spectral bands has been described in our earlier papers [5][6]. Here we provide a brief summary in the context of linear unmixing.

The N bands (centred at wavelengths λ_k , $k=1, \dots, N$) are chosen through optimisation. The optimisation process uses a set of simulated spectra generated from the library spectra $\{\mathbf{L}\}$ and a set of coefficients $\{\mathbf{A}\}$ according to equation (2). Coefficients in $\{\mathbf{A}\}$, $a_{mn} \in [0,1]$, are chosen to represent a range of different mixtures of the constituent fluorescent compounds.

The set $\{\mathbf{S}\}$ of spectra generated in this way represents the 'pure' fluorescent emissions. The effects of the imaging system are then incorporated by including the camera quantum efficiency, $Q(\lambda)$, the filter transmission at the acquisition wavelengths, $F_k = F(\lambda_k)$, and by incorporating noise drawn from Poisson distribution [6][7] (its 'addition' denoted by \otimes). Thus the recorded image spectra $\{\mathbf{S}'\}$ are given by

$$\mathbf{S}' = \mathbf{S} \cdot \mathbf{Q}^T \cdot \mathbf{F}^T \otimes \varepsilon, \quad \varepsilon = \sqrt{(\mathbf{S}' + \mathbf{D} + \mathbf{N}^2)} \quad (4)$$

\mathbf{D} is the camera dark current and \mathbf{N} is the camera readout noise. It should be noted that in the above $K=N$, i.e. the number of spectral measurements K is equal to the number of fluorochromes N .

The objective of optimisation is to find N acquisition wavelengths F_k such that:

1. the solution to $\mathbf{A}' = \mathbf{L}^{-1} \cdot \mathbf{S}'$ is unique; and
2. the solution minimises the error with which the abundance coefficients \mathbf{A}' are recovered (\mathbf{A}' -s are estimates of \mathbf{A} -s).

The first condition is met if the determinant of the Jacobian matrix

$$\mathbf{J} = \begin{bmatrix} \frac{\partial \mathbf{S}'}{\partial \mathbf{A}'} \end{bmatrix} \quad (5)$$

$\det(\mathbf{J})$ is either strictly positive or strictly negative over the whole domain of \mathbf{A} [5]. As there may be many solutions

satisfying the first condition, the second condition allows one to select those F_k -s for which the difference

$$|\mathbf{A}' - \mathbf{A}|, \mathbf{A}' = \mathbf{L}^{-1} \cdot \mathbf{S}' \quad (6)$$

is minimised. It is possible to compute the difference in the equation (6) because the abundance coefficients \mathbf{A}' , used to generate the simulated spectra, are known.

B. Unmixing with a reduced number of spectral measurements

On the completion of the optimisation process we obtain the definitions of N acquisition wavelengths F_k . Image measurements at these wavelengths will enable us to obtain the estimated abundance coefficients \mathbf{A}' characterising the magnitudes of the library spectra \mathbf{L} :

$$\mathbf{A}' = \mathbf{L}^{-1} \cdot \mathbf{I} \quad (7)$$

where \mathbf{A}' is a $N \times M$ matrix, \mathbf{L}^{-1} is a $N \times N$ matrix and \mathbf{I} is a $N \times M$ matrix.

The difference between equation (7) above and equation (3) is that the abundance parameters are computed using the number of spectral measurements equal to the number of fluorescent compounds present in the sample. As stated in the introduction, this has a potential of significantly reducing the acquisition times required for imaging of multiple fluorochromes.

IV. VERIFICATION AND VALIDATION

The use of a significantly smaller number of measurements may reduce the accuracy of the coefficients obtained by unmixing. We have carried out a number of experiments to determine the magnitude of this potential loss of accuracy for mixtures of up to three fluorochromes.

A. Verification using simulated image data

The method was first validated on simulated image data constructed as follows. Two existing library spectra of length $K > N$ and with overlapping emissions were used. The abundance coefficients for each spectrum at each image point were defined by values in N image matrices (see fig 2(a)-(c)). A multispectral image \mathbf{I} of size $K \times M$ was computed by using equation (2), where A_n - s were taken from the matrix n . At each image point noise drawn from Poisson distribution was added to the spectrum.

To obtain coefficients \mathbf{A} from the simulated image, spectral values were obtained at the N optimal wavelengths λ_n and coefficients \mathbf{A}' were computed using equation (7). The RMS error was then computed at each image point. Additionally, the estimated image values were computed for the full range of the wavelengths, K , by reconstructing the image spectra from the coefficients \mathbf{A}' and the full library spectra \mathbf{L} :

$$\mathbf{I}' = \mathbf{A}' \cdot \mathbf{L} \quad (8)$$

The discrepancy between the original and the reconstructed spectra was measured by computing

$$\text{RMS} (|\mathbf{I} - \mathbf{I}'|) / \max(\mathbf{S}). \quad (9)$$

B. Validation of the method using real image data

In contrast with the simulated data, the ground truth data in the form of coefficients \mathbf{A} is not available for real images. However, it is still possible to estimate the accuracy of the solution by reconstructing the estimated spectra and comparing them to the measured spectra, as in equation (9). In this instance a small error does not guarantee that the coefficients are correct (analysis of this aspect is presented in a forthcoming paper); however, a large error always indicates a problem.

C. Comparison using full spectral data

The abundance coefficients computed with the minimum number of spectral bands were compared to the values obtained using a commercial system Nuance (C.R.I.) which implements linear unmixing with the full image spectra [8].

V. IMAGING EXPERIMENTS

A. Materials

Experiments were performed to determine the ability of our new method to separate different fluorochromes in a mixed population. This was achieved in two ways: using commercially available slides containing mixed populations of fluorescent beads (Molecular Probes, FocalCheckTM Slide 2 F36913, Invitrogen, Paisley, UK), and using slides containing cells labelled with different fluorochromes.

The beads come in two varieties: in one each bead is labelled with a single fluorochrome, and a bead population contains two types of beads with closely overlapping emission spectra; in the other the outer ring and the core of each bead is labelled with different fluorochromes, also with closely overlapping spectra. In the experiments we have used beads A1 and B1 which fluoresce in green at CW=511nm and 524nm respectively (see fig. 1(a)).

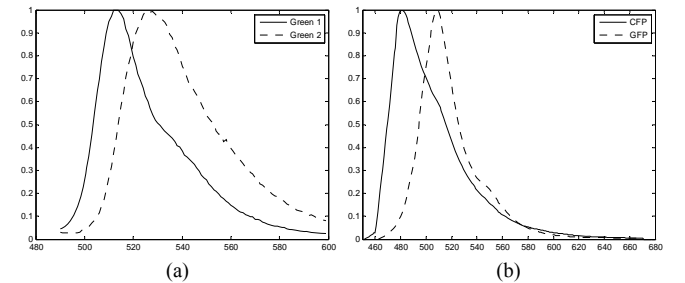


Fig.1: (a) Emission spectra for green fluorescent beads with central wavelengths (CW) of 511nm (Green 1) and 524nm (Green 2); (b) Emission spectra for fluorescent proteins CFP and GFP. Both sets of spectra show significant overlap.

In the experiments using cells two fluorochromes were present: CFP and GFP (see fig 1(b) for the library spectra). The slides were prepared by mounting fixed cells containing

the fluorochromes in Prolong Gold Antifade (Molecular Probes P36930, Invitrogen) in the absence of DAPI. RBL-2H3 cells were transfected with 20 μ g combinations of DNA for each fluorochrome. Fluorochromes were properly expressed in cells after 16 hours. Cells were then fixed by treatment in 4% paraformaldehyde for 10minutes, washed in a physiological salt solution and mounted in Prolong Gold.

B. Imaging methods and equipment

The slides were imaged on a Nikon TE300 inverted microscope using mercury lamp illumination and a filter cube comprising two filters: the excitation filter (bandpass, 400-440nm) and the dichroic mirror filter (longpass, 455nm). Images were acquired using a Cambridge Research Instruments Nuance system mounted on the camera port of the microscope. The Nuance system incorporates VariSpec filters (range 400-720nm, width 10nm) and a high-sensitivity monochrome camera. Calibration curves incorporating camera quantum efficiency and filter transmission as a function of wavelength were obtained by imaging SpectralonTM calibration tiles.

The full spectra were acquired at 30 wavelengths in the spectral range between 460 and 680nm. The reduced spectra were acquired at 3 wavelengths; the optimal filters used in the experiments are listed in Table I. Acquisition times per spectral wavelength were of the order of 10-100 msec for the beads and 5 sec for the cells.

TABLE I
OPTIMAL FILTERS USED FOR IMAGE ACQUISITION

	λ_1	λ_2	λ_3
Flourescent beads	510	530	568
CFP/GFP	488	508	544

C. Pre-processing and analysis

The image data acquired in the experiments includes the effects of the filter transmission and the camera quantum efficiency, as shown in equation (4). These are known from the system calibration and were removed, so that only the emission data was the subject of the analysis.

The library spectra used for unmixing were kindly provided by Dr R.M.Zucker [9] for the beads; those for the fluorescent proteins CFP and GFP were obtained from technical publications of Molecular ProbesTM. The library spectrum for the combined background fluorescence and autofluorescence was constructed by averaging spectral emissions from the slides prepared as described above but containing only non-transfected cells.

VI. RESULTS

A. Simulated image data

The real spectra of the green fluorescent beads (see fig. 1(a)) were used as the library spectra; the background was set to a constant. The abundance coefficients for each spectrum at each image point were defined by values in 3 image matrices

(see fig. 2(a)-(c)). Figure 3(a) shows a slice from a computed multispectral image at $\lambda = 518$ nm where the overlap between the two library spectra is at its maximum. Noise can be clearly seen. Plot in figure 3(b) shows the original (noiseless) spectrum at a pixel in the centre of the image (where the two spectral emissions overlap) together with the spectrum with the added Poisson noise. The corresponding maps showing the abundance coefficients computed from the noisy multispectral image data using 3 wavelengths are shown in figure 2(d) - (f). The reconstructed spectrum corresponding to the noisy image spectrum in the centre of the image is shown in figure 3(b). The mean values and RMS errors for each of the simulated fluorescent compounds are given in Table II.

Without the added noise the abundance coefficients were recovered perfectly (RMS around $0.5 \cdot 10^{-14}$).

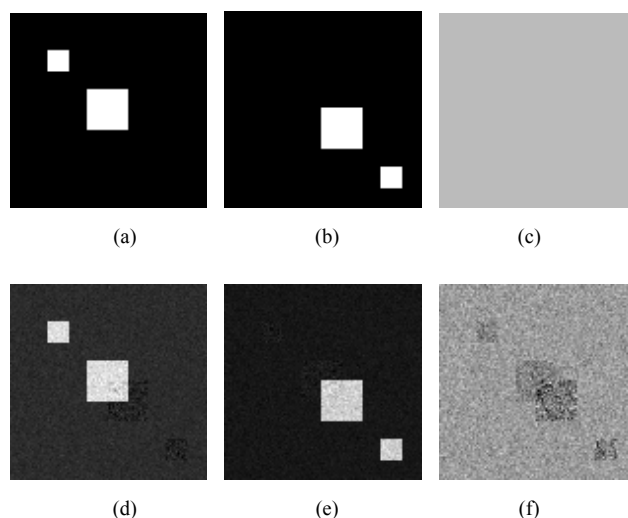


Fig. 2: (a) A spatial map of the fluorescent compound 1 to be used with the library spectrum L_1 ; dark region has value 0, bright regions have value 2. (b) A spatial map of the fluorescent compound 2 to be used with the library spectrum L_2 ; dark region has value 0, bright regions have value 3. (c) A spatial map of the background, set to a constant value of 1. (d)-(f) Reconstructed spatial maps of the fluorescent compounds 1, 2 and the background, respectively

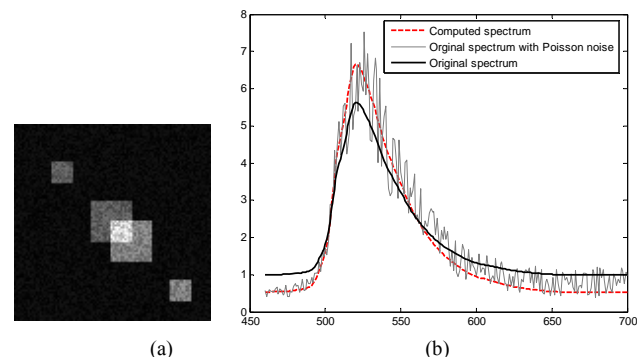


Fig. 3: (a) One slice, at $\lambda = 518$ nm, of the simulated fluorescent emission image with Poisson noise added. (b) Plot showing the original (noiseless) spectrum at one point in the centre of the image (solid black line), spectrum at the same location with noise added (grey thin line), and the spectrum reconstructed from noisy data (dashed red line).

TABLE II

RESULTS FOR THE SIMULATED FLUORESCENT COMPOUNDS

Component	1		2		B		E
	A	A'	A	A'	A	A'	
1+B	2	2.3	0	0.06	1	0.96	0.18
2+B	0	0.2	3	2.92	1	0.9	0.08
B	0	0.12	0	0.02	1	1.03	0.12
1+2+B	2	2.23	3	2.96	1	0.82	0.06

Component: components present at a given location; for example in the top left square the fluorescent component 1 is overlaid on the background component B. A and A' : the given and the recovered abundance coefficients; E: RMS/max(S) error.

B. Beads

Figure 4 shows a colour image of two different green fluorescent beads together with the pictorial results of spectral unmixing obtained from 3 measurements. The results using the full spectra were very similar as demonstrated in figure 4(d) which shows the nearly perfect overlap between the profiles of the abundance coefficients obtained using the two different methods. A typical RMS difference between the two methods has the mean of 0.007 and the maximum of 0.031.

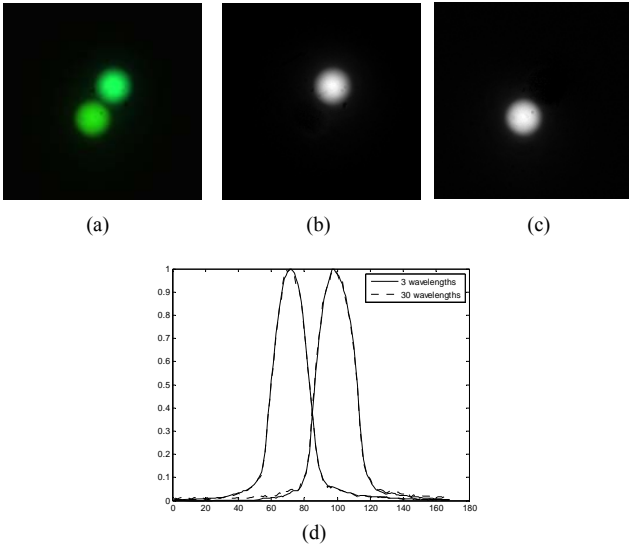


Fig. 4: (a) True colour representation of a multispectral image of two different green fluorescent beads, the top one is of the type Green 1 (emission spectrum with CW=511nm), the bottom one is of the type Green 2 (emission spectrum with CW=224nm). (b) and (c) show the pictorial results of linear unmixing applied to the multispectral image in (a); the image brightness corresponds to a normalized abundance coefficient for Green 1 (figure b) and Green 2 (figure c). (d) The plots show the profiles through the centres of the two beads (Green 1 on the right and Green 2 on the left). The normalized abundance coefficients recovered from 30 wavelengths using a conventional linear unmixing are shown in dashed lines, those recovered using 3 wavelengths are shown in solid lines.

Figure 5(a) shows a colour image of a fluorescent bead composed of two different fluorescent dyes with closely overlapping spectra. The pictorial results of spectral unmixing obtained from 3 measurements are shown in 5(b) and 5(c) and clearly demonstrate the ability of the method to separate the contributions of the two dyes. Some spatial overlap in the contributions from the ring and the core is due to the fact that the microscopy images are not confocal, i.e. they contain

emissions from the outside of the plane of focus. Figures 6(a) and (b) show the comparison between the normalized coefficients obtained using the 3 optimal wavelengths with those using the full 30-wavelength range and implemented in the Nuance system. Figures 6(c) and (d) show the relative contributions from the dyes contained in the ring and in the core of the bead. The RMS difference between the two methods has the mean of 0.009 and the maximum of 0.027.

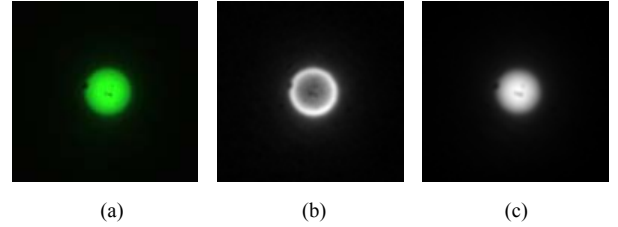


Fig. 5: (a) True colour representation of a multispectral image of a fluorescent bead composed of two different fluorescent dyes: the outer ring is of the type Green 1 (emission spectrum with CW=511nm), the inner core is of the type Green 2 (emission spectrum with CW=224nm). (b) and (c) show the pictorial results of linear unmixing applied to the multispectral image in (a); the image brightness corresponds to a normalized abundance coefficient for Green 1 (figure b) and Green 2 (figure c).

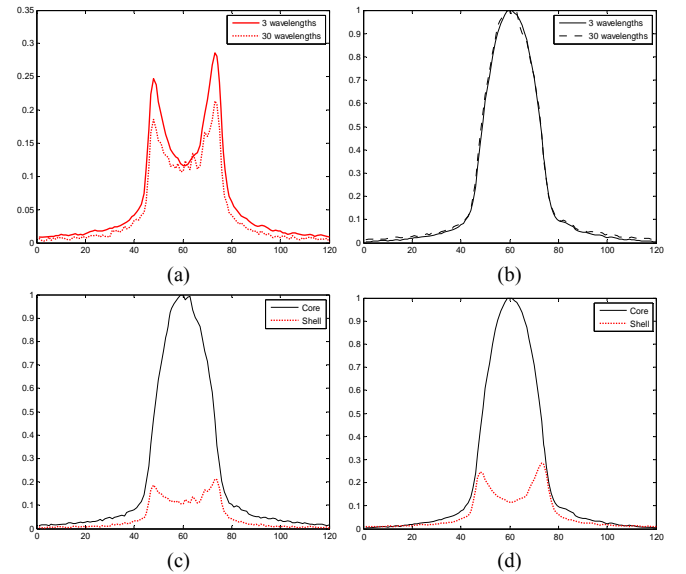


Fig. 7: The profiles through the centre of the bead shown in figure 5(a). The plots show the magnitudes of the normalized abundance coefficients for Green 1 (the outer ring) and Green 2 (the inner core). (a) The comparison of the normalized abundance coefficients recovered from 30 wavelengths using a conventional linear unmixing (dotted lines) and using 3 wavelengths (solid lines) for Green 1. (b) The comparison of the normalized abundance coefficients recovered from 30 wavelengths using a conventional linear unmixing (dashed lines) and using 3 wavelengths (solid lines) for Green 2. (c) The relative magnitudes of normalized abundance coefficient recovered using 30 wavelengths for the outer ring and the inner core. (d) The relative magnitudes of normalized abundance coefficient recovered using 3 wavelengths for the outer ring and the inner core.

C. Cells

Figure 7 illustrates the results of spectral unmixing applied to multispectral images of a cell transfected with two fluorescent proteins: CFP and GFP. Abundance coefficients are computed for these proteins and also for the background-

and auto-fluorescence and shown in pictorial form in figures (b)-(d) and (f)-(g). The results in (b)-(d) are obtained from 30 measurements using the Nuance system; those in (f)-(g) are obtained from 3 measurements using our method. All the images are contrast-stretched. Qualitatively the results are similar, although the differences can be observed in the overall balance of the magnitudes, and particularly in the locations at which the presence of GFP was detected. Figure (e) shows pictorially the normalized RMS error at each point between the measured spectrum (at 30 wavelengths) and the spectrum reconstructed from 3 measurements (see equation (9)). Quantitatively, the mean normalized RMS error for this image was 0.037, the maximum normalized RMS error was 0.169; the respective non-normalised values (i.e. not divided by $\max(\mathbf{S})$ in equation (9)) were: mean 0.014, maximum 0.095. On a set of 10 images the mean RMS error was in the range 0.02-0.09.

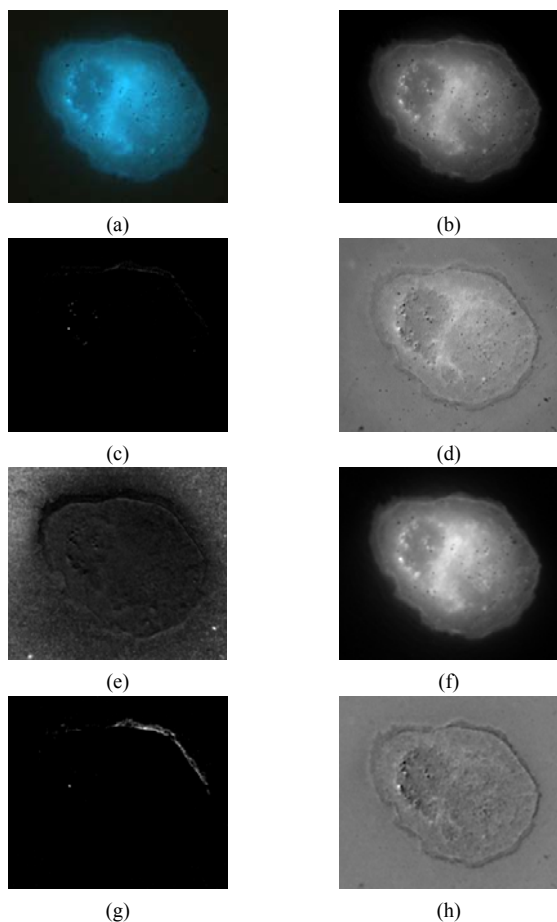


Fig. 7: (a) True colour representation of a multispectral image of an RBL-2H3 cell transfected with two different fluorescent proteins, CFP and GFP (see text). (b), (c) and (d) show the pictorial results of the conventional linear unmixing with 30 wavelengths applied to the multispectral image in (a); the image brightness corresponds to a normalized abundance coefficient for CFP (figure b), GFP (figure c) and background- / auto-fluorescence (d). (f), (g) and (h) show the equivalent pictorial results of the linear unmixing with the 3 optimal wavelengths applied to the multispectral image in (a); the image brightness corresponds to a normalized abundance coefficient for CFP (figure f), GFP (figure g) and background- / auto-fluorescence (h). (e) Pictorial representation of the $\text{RMS}/\max(\mathbf{S})$ error (see text and equation (9)).

Examples of the 30-wavelength measured spectra and the corresponding spectra reconstructed from 3 measurements at the optimal wavelengths for the data in figure 7(a) can be seen in figure 8. The plots show spectra for different combinations of the abundance coefficients for CFP, GFP and the background- and auto-fluorescence, as listed in Table III. Plot number 4 shows a pair of spectra at a point with the largest RMS error.

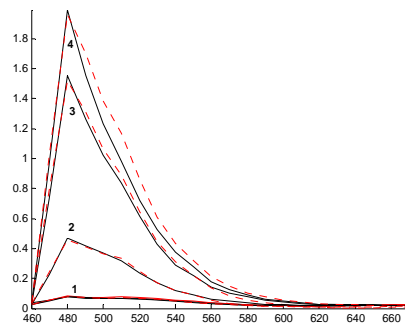


Fig. 8: Four examples of the original 30-wavelength spectra obtained directly from the original multispectral image in figure 7(a) (solid line) plotted against the spectra reconstructed from the three measurements at 488, 508 and 544 nm (see Table I) and the three library spectra (CFP, GFP and background- / auto-fluorescence) according to equation (8). Table III shows the relative abundances corresponding the above spectra (AU).

TABLE III
RELATIVE ABUNDANCE FOR THE EXAMPLE SPECTRA

Spectrum number	CFP	GFP	Background / Autofl.
1	0.1	0	0.2
2	0.9	0.1	3.4
3	3.1	0	0.3
4	3.9	0	6.8

VII. CONCLUSIONS AND DISCUSSION

We have demonstrated that, in principle, adequate spectral unmixing of N fluorochromes can be obtained using only N spectral measurements. Traditional methods typically use $K \gg N$ measurements for this.

On simulated spectra with no added noise the recovery is perfect. On the spectra with the heavy Poisson noise the $\text{RMS}/\max(\mathbf{S})$ error is under 20% for the components whose abundance is low in comparison to the background fluorescence, and under 12% for the remaining components, even in the presence of substantial spectral overlap.

On real data, where ground truth is not available, the differences between our method and a full linear unmixing are minimal, as demonstrated in the experiments using fluorescent beads (mean $\text{RMS} < 0.009$) and real cells (mean $\text{RMS} < 0.037$). Qualitative differences between the coefficients recovered for the real cells are very small.

Although we have not carried out numerical experiments probing the sensitivity of the method to the precise choice of the acquisition wavelengths F_k , our observations suggest that small differences, of the order of $\sim 5\text{nm}$, do not seem to affect the accuracy of the recovered parameters.

The proposed method has a clear advantage in that it the acquisition of N wavelengths for N components is likely to take much less time than the acquisition of the full spectral range. This reduces the amount of bleaching and also supports the dynamic studies. The only additional data required for the use of this method is the system calibration data; and the only additional processing required is the computation of the optimal wavelengths, which is of the order of several minutes for three spectral components and needs to be done only once for a given imaging system and a given combination of fluorochromes.

ACKNOWLEDGMENTS

This research was funded by the Medical Research Council (UK) grant MRC/77520. The authors wish to thank Dr R.M.Zucker for the spectral libraries of the fluorescent beads.

REFERENCES

- [1] Shirakawa H, Shunichi Miyazaki S (2004) Blind Spectral Decomposition of Single-Cell Fluorescence by Parallel Factor Analysis *Biophysical Journal* 86, 1739-1752.
- [2] Chang C-I, Chiang S-S, Smith, JA, Ginsberg IW (2002) Linear spectral random mixture analysis for hyperspectral imagery. *IEEE Trans. Geoscience and Remote Sensing* 40 (2), 375-392.
- [3] Mansfield JR et al (2005) Autofluorescence removal, multiplexing, and automated analysis methods for in-vivo fluorescence imaging. *Journal of Biomedical Optics* 10(4), 041207-1 - 041207-9.
- [4] Hyvärinen A, Karhunen J, Oja E. *Independent Component Analysis*. John Wiley & Sons, 2001.
- [5] Preece SJ, Claridge E (2004) Spectral filter optimisation for the recovery of parameters which describe human skin. *IEEE Pattern Analysis and Machine Intelligence*, 26(7), 913-922.
- [6] Claridge E, Powner D, Wakelam M (2006) The analysis of fluorescence microscopy images for FRET detection. MICCAI06, *Workshop on Microscopic Image Analysis with Applications in Biology*. Metaxas DN, Whitaker RT, Rittcher J, Sebastian T (Eds), Copenhagen, October 2006, 39-45.
- [7] Cheezum MK et al (2001) Quantitative comparison of algorithms for tracking single fluorescent particles. *Biophysical Journal* 81, 2378-2388.
- [8] Levenson RM, Mansfield JR (2006), Spectral Imaging in Biology and Medicine: Slices of Life. *Cytometry A* 69(8), 748-58.
- [9] Zucker RM et al (2007) Reliability of confocal microscopy spectral imaging systems: use of multispectral beads. *Cytometry Part A* 71A, 174-189.